Nanoscale Aggregation of Cellular β_2-Adrenergic Receptors Measured by Plasmonic Interactions of Functionalized Nanoparticles

David C. Kennedy,[†] Li-Lin Tay,[‡,*] Rodney K. Lyn,[†] Yanouchka Rouleau,[†] John Hulse,[‡] and John Paul Pezacki[†,*]

[†]Steacie Institute for Molecular Sciences, National Research Council of Canada, 100 Sussex Drive, Ottawa, Canada K1A 0R6, and [‡]Institute for Microscructural Sciences, National Research Council of Canada, 1200 Montreal Road, Ottawa, Canada K1A 0R6

ABSTRACT Adrenergic signaling that controls the contraction of cardiac myocyte cells and the beating of the mammalian heart is initiated by ligand binding to adrenergic receptors contained in nanoscale multiprotein complexes at the cellular membrane. Here we demonstrate that the surface-enhanced Raman scattering (SERS) of functionalized silver nanoparticles can be used to report on the receptor aggregation state of specifically label β_2-adrenergic receptors on mouse cardiac myocyte cells. Furthermore, multimodal imaging including Raman, Rayleigh scattering, scanning electron microscopy, and luminescence imaging was combined to fully characterize the β_2-adrenergic receptor-mediated aggregation of silver nanoparticles on the membrane of cardiac myocytes. Scanning electron microscopy analysis reveals distinct SERS active clusters of between 10 and 70 nanoparticles per signaling domain from ultra-high-resolution images of β_2-adrenergic receptor clusters on the cellular membrane. These techniques can be generally applied to study the aggregation of other cell surface receptors and explore their distribution on cell surfaces.

KEYWORDS: plasmonic nanoparticles · surface-enhanced Raman scattering · cell receptors · aggregation · multimodal imaging

Adrenergic signaling controls the beat rate in the mammalian heart and involves the binding of catecholamines including adrenaline to β-adrenergic G-protein-coupled receptors (βARs) on cardiac myocytes.[1−4] Establishing a receptor density/oligomerization state with the signaling complexes on cells at the nanoscale remains challenging, thus highlighting the need for alternative ways to study their density and aggregation states.[5−7] On mouse cardiac myocytes, functional β-adrenergic receptors are organized into small signaling domains of ~140 nm average size that contain on average 12−72 receptor molecules.[7] Functional βARs are associated with multiprotein complexes called signalosomes that include the α, β, and γ G-protein subunits and either the β_1 or β_2 isoform of βAR.[3,8,9] It appears that receptor aggregates form and give rise to nanoscale signaling platforms,[7] although it is not clear whether these aggregates represent higher densities of membrane proteins in membrane rafts or whether they form due to protein−protein interactions in the cell membrane.[5,6] Recent methodologies have identified oligomeric states of four or more β_2ARs on cardiac myocytes, but the elucidation of the structures that form larger aggregates that are responsible for signaling still remains a critical challenge in understanding receptor activity.[10] X-ray crystallography has revealed that the structure of the β_2AR and its seven transmembrane spanning helices give it a topology that is nanometer in scale.[11,12] Structural studies,[13] Förster resonance energy transfer (FRET),[14] and bioluminescence resonance energy transfer (BRET)[9,15] experiments indicate that agonist binding results in local conformational changes and small scale reordering of the local protein environment on scales of less than 10 nm. The landscape of receptors on the cell surface appear to be driven by local membrane environments such as rafts, and these features are of tens to hundreds of nanometers, a larger scale than can be measured by resonance energy transfer techniques but are below the diffraction limit, making them too small to be observed by confocal microscopy.[5,6] Homo- and heterodimers and oligomers have been implicated in signaling using these methodologies;[9,15−18] however, the larger scale presentation and ordering of the receptors into signaling clusters could not be probed, nor the size of oligomers accurately determined. Also, such methods rely on overexpression systems that may alter their presentation on

*Address correspondence to lilin.tay@nrc-cnrc.gc.ca, john.pezacki@ nrc-cnrc.gc.ca.

Received for review May 12, 2009 and accepted July 20, 2009.

Published online July 27, 2009.
10.1021/nn900488u CCC: $40.75

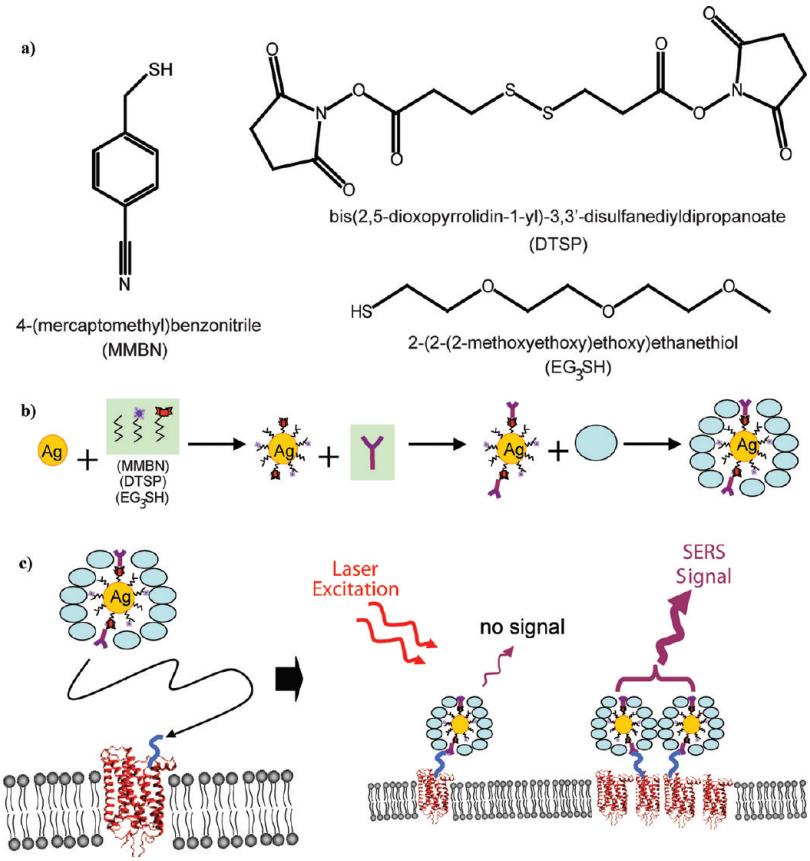

Figure 1. Molecular structures of the functionalized silver NPs for cell surface labeling. (a) Molecular structures of the ligands used to coat the nanoparticles. (b) Schematic depiction of the synthesis of functionalized Ag NPs. Colloidal Ag sol is first reacted with a mixture of two thiol and one disulfide containing molecules, then activated with an antibody, followed by blocking on the remainder of the particle with BSA (BSA is not labeled in the figure). (c) Particles bind to the cell surface receptors *via* the covalently linked antibody and are then imaged with a Raman microscope.

the cell surface from what was naturally displayed and/or disruption of the membrane to quantify dimers.[19] Targeted imaging of the naturally occurring receptor distribution can be facilitated by using antibody-labeled metal nanoparticles (NPs).[20−26] Appropriately functionalized metal NPs have been used extensively to examine biomolecular aggregates,[20−26] and we have shown recently that cell surface receptors can function as clusters and that these clusters can, in turn, help to facilitate nanoparticle (NP) aggregation giving rise to intense surface-enhanced Raman scattering (SERS).[27] Functionalized nanorods have been used to target EGFR on cancer cells to identify tumor cells using two-photon luminescence and SERS.[21,28] However, nanorods are not ideally suited for reporting on membrane protein aggregation because their shape allows them to interact with multiple receptors at the same time. SERS microscopy is an ideal technique to probe the cell surface receptor aggregation. Ag and Au NPs generate readily observable SERS signal through the capacitive enhancement from the coupled nanostructures aided by receptor aggregation. This provides a direct route to monitor the clustered receptors on the cell surface. Here we demonstrate an optimized strategy of NP labeling that allows SERS imaging of β-adrenergic receptor complexes and quantification of the size of β_2AR aggregates in the signalosome. In addition, we also demonstrate the ability to identify unique local environments associated with active protein complexes.

RESULTS AND DISCUSSION

Functionalized Nanoparticles and Receptor Aggregation. In developing methods for SERS imaging of β_2AR aggregates, we first considered the optimal design of the NP ligands for β_2AR labeling. Practical considerations of water solubility, simplified functionalization, as well as the proximity and orientation of the Raman reporter to the NP surface were carefully considered for optimal SERS imaging of membrane protein aggregation states (Figure 1). Nitriles are excellent Raman reporters in that their CN[29] resonance is distinct from those of the cell.[30] The nitrile functional group exhibits a Raman vibrational band at ~2200 cm^{-1} that falls in a spectroscopically silent region of the Raman spectrum of a cell[30] and most of the commonly used ligands for passivation and antibody cross-linking. Here we chose to use one of the simplest nitriles to functionalize the NP, 4-(mercaptomethyl)benzonitrile (MMBN)[31] (Figure 1a). In contrast to other dye-based Raman reporter mol-

ecules, MMBN is robust and unlikely to undergo photodegradation.

In addition to selecting an effective reporter molecule, the other ligands were also selected for their simplicity and functionality (Figure 1a). Dithiobis(succinimidyl propionate) (DTSP) can be reduced *in situ* by the NP surface to form two coordinated thiols on the NP, providing the necessary functional group (succinimide ester) for further antibody conjugation.[32] This was found to proceed quickly (30−60 s) and was always performed first before the addition of other thiol ligands. 2-(2-(2-Methoxyethoxy)ethoxy)ethanethiol (EG_3SH) (Figure 1a) is a simple PEGylated thiol that has been previously shown to coordinate to metal NPs to form water-soluble particles[33] and was used here as a water-soluble space filling as well as passivation ligand on the surface of the NPs. Addition of more than 50% of MMBN (of all thiolated ligands used in the NP functionalization) resulted in particles that were insoluble upon resuspension in PBS or water. We have previously shown that the coverage of the surface is roughly proportional to the ratio of thiols added.[27] The ligand ratio used in the above-mentioned protocol was carefully tailored to produce monodispersed functional NPs for further protein conjugation. The SERS spectrum of the MMBN functionalized particles (Figure 2a) exhibits three dominant vibrational features with a doublet of 1180 and 1226 cm^{-1} due to the in-plane C−H bending mode, a strong sharp band at 1609 cm^{-1} from the in-plane aromatic ring deformation, and a band at 2220 cm^{-1} from the nitrile stretching mode.[34] The detailed experimental protocols for NP synthesis are provided in the Materials and Methods section below.

Next we considered the optimal NP size for β_2AR imaging. Here we chose NPs of similar size to that of the membrane protein receptor, so that each receptor would be labeled by ~1 NP. The absorption and scattering properties of the metallic NPs are dominated by the optical resonances due to the collective excitation of the conduction electrons, known as the localized surface plasmon resonance (LSPR),[35−37] which is responsible for the intense signals observed in the surface-enhanced linear and nonlinear spectroscopies. SERS has been applied to achieve ultrahigh sensitivity detection in many bioanalytical assays as well as in different types of cell imaging studies.[20−26]

The structure of β_2AR in the membrane likely spans 4−5 nm in diameter based on existing crystal structures,[11−13] and typical signaling platforms are ~140 nm in diameter on the cell surface.[7] Also, β_2ARs are thought to form cholesterol-mediated homo- and heterodimers within the membrane, and it is reasonable to assume that such protein complexes could have a diameter of 10 nm or greater.[38] Therefore, NPs 50 nm or larger in diameter, such as those typically employed in SERS microscopy,[27,39] are not suitable to study receptor aggregation. Ideally, the aggregation can be best probed if the receptors are labeled with NPs of similar size to that of the receptors so that when the receptor oligomerizes so too do the NPs. The SERS enhancement observed from the tightly coupled NPs can be orders of magnitude larger than the monodispersed NPs.[40] In the coupled systems, the enhancement is strongly dependent on the separation of the coupled nanostructures.[40] Labeling with NPs that are smaller than the average size of β_2AR will likely not generate observable SERS signals even at sites of receptor aggregation due to insufficient LSPR coupling. Hence 15 nm Ag particles, characterized by transmission electron microscopy (TEM) (Supporting Information, Figure S1), were chosen as an optimal size to generate SERS signal *via* coupling of their LSPRs yet are still small enough to report on nanometer-sized protein structures. Although the reduction in the particle size poses a penalty on the overall SERS enhancement, intense SERS signal generated from the coupling of NPs (through the capacitive enhancement of their coupled LSPRs) enables the observation of receptor aggregates rather than single receptors on the cell surface. In fact, our choice of NP was to allow for the treatment of cells with monodispersed NPs functionalized with antibodies to specifically target β_2AR so that the SERS signal would essentially report on the clustered states of the cell surface receptors.

SERS Imaging of Aggregated Adrenergic Receptors. In our studies of β_2AR, we have attempted new methods for developing a global understanding of receptor localization and aggregation in order to understand how these phenomena may contribute to signaling events that control the beat rate of the mammalian heart. Mouse cardiomyocyte cells were first treated with commercially available β_2AR antibodies (Ab) using a protocol established in our earlier studies.[7] Specific labeling of β_2AR was achieved with the EG_3SH-, MMBN-, and DTSP-activated NPs conjugated to a secondary Ab. Control experiments were performed with cells that lack the primary antibody treatment and NPs that lack the secondary Ab conjugation. The control experiments showed primary Ab-treated cells exposed to NPs without the secondary Ab, and cells not treated with the primary Ab but treated with fully functionalized NPs with the secondary Ab gave cells with no NP attachment to the cell membrane, which indicates that NP labeling is specific for β_2AR under the appropriate conditions (Supporting Information, Figure S1). We emphasize that cells were washed three times with PBS before imaging to remove any unbound particles and that no free particles are ever observed in solution. Additional washing did not effect the intensities of the observed signals across all experiments, suggesting that the NP−receptor adducts are sufficiently robust to survive the sample preparation. Recently, monoclonal antibodies have been developed to improve the efficacy and selectivity of Ab binding for β_2AR;[41] however, this spe-

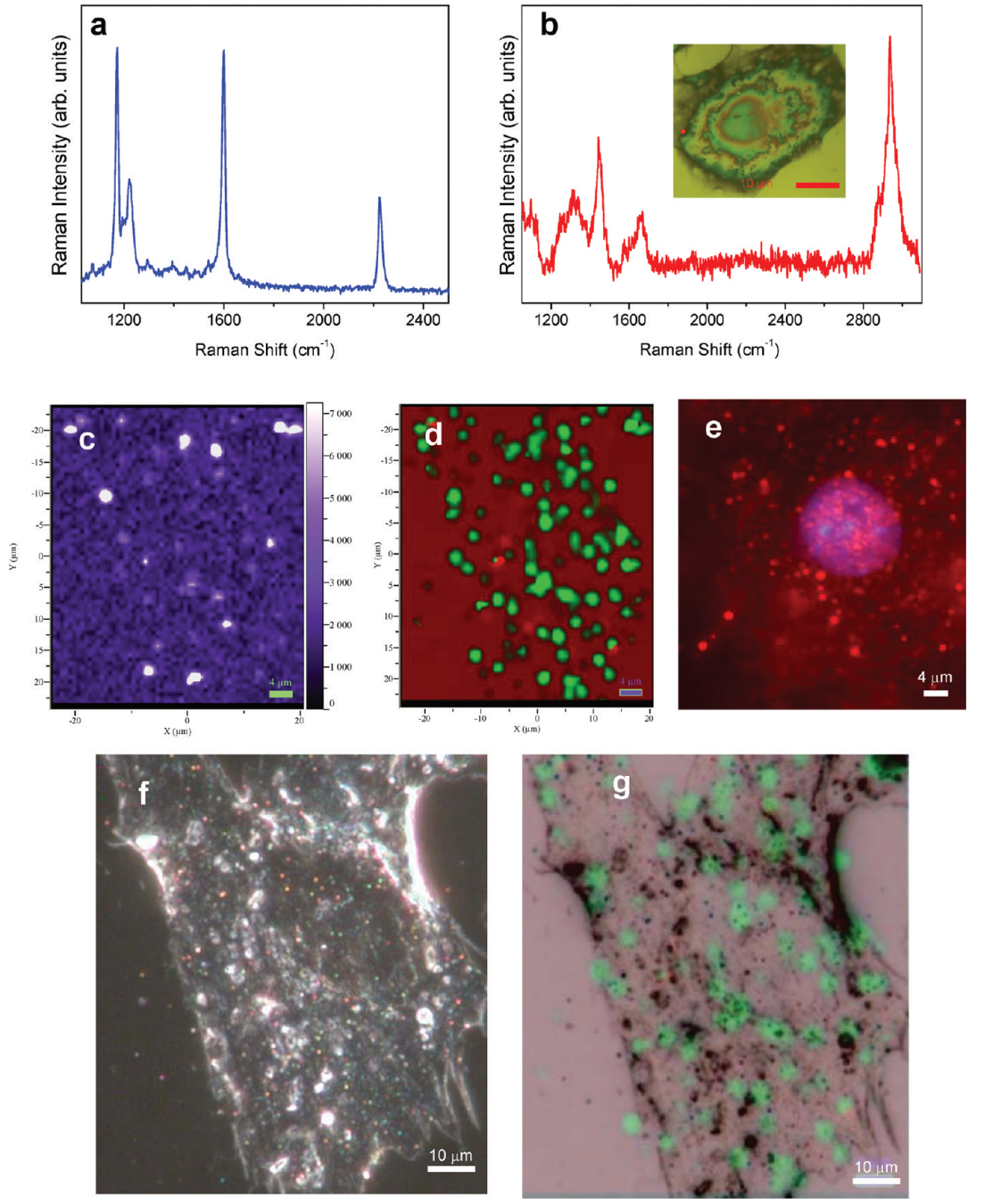

Figure 2. SERS imaging of H9c2 cardiac myocytes. (a) SERS spectrum of MMBN Raman reporter molecule. (b) Cell Raman spectrum taken from the nucleus region of the cell shown in the inset. (c) SERS image of the normalized CN intensity map of a fixed H9c2 cell immunostained for β_2AR and co-stained with secondary antibody-functionalized NPs. (d) Multivariate deconvolution of the MMBN SERS spectra for fixed H9c2 cells immunostained for β_2AR and co-stained with secondary antibody-functionalized NPs. (e) Different cell labeled by conventional fluorescent antibody staining. (f) Rayleigh light scattering image of the corresponding H9c2 cell shown in (c) and (d). (g) Overlay of (d) and (f) deconvolution map overtop of Rayleigh light scattering image. Small colored spots in (f) correspond well with SERS active sites (green spots) for NPs from (d).

cific polyclonal Ab has been used to selectively target β_2ARs on cells.[42]

A strong SERS signal of the C≡N band can be observed upon specific binding (Figure 2a). The most intense SERS spots appear to arise from larger aggregates of β_2AR that mediate NP aggregation. Normalized C≡N SERS intensity maps of the NP-treated cells typically show areas with strong SERS signal for aggregated β_2AR. These normalized features were observed to be uniformly spread across the cell surface and separated by ~5 to 10 μm (Figure 2c and Supporting Information, Figure S2). The normalized C≡N intensity map (Figure 2c) is dominated by ~10 extremely intense spots, where the C≡N band intensity is ~50 times higher than the weaker (yet observable spectra) MMBN spectra. Deconvolution using multivariate analysis gener-

ated a more universal distribution of the MMBN, which is consistent with our earlier immunofluorescence studies of the same receptor[7] (Figure 2d and Supporting Information, Figure S3).

Multimodal Imaging of NP-Labeled Adrenergic Receptors on Cell Surfaces. One benefit of using noble NPs to study receptor binding phenomena is that they can also be probed with a variety of compatible imaging techniques. The plasmonic nature of the NP results in a wavelength selective absorption and scattering with extremely high efficiency.[37,40] For example, a 60 nm Au NP is brighter than 10^5 typical small molecule fluorophores such as fluorescein.[43] The sensitivity of its index of refraction to its immediate environment has also been exploited in the monitoring of molecular binding events as well as nanosensor applications.[26,36,44,45] The resonant Rayleigh scattering of a single NP cluster is easily observed using a dark-field optical scattering microscopy setup. Here, we have also used Rayleigh light scattering to generate high-resolution images of the Ag NPs and probe the NP (and thus, receptor) distribution on the cell surface. While monodispersed silver NPs scatter light at ~405 nm, aggregation due to the receptor clustering can result in a red shift of their LSPR and increase in the scattering intensity. The Rayleigh light scattering image of a NP-treated cell is shown in Figure 2f, where the bright colored spots represent the Ag NPs, clearly distinguishing them from salt and other features that may be scattering light on the cell surface. In order to quantify the NP distribution on the cell surface, we imported the Rayleigh light scattering data into image processing software that deconvoluted the data and counted the NPs from the optical image (Figure 3). The deconvoluted NPs appeared as circular halo-like features which can be easily discerned from other surface features such as salt or cell organelles. These halo-like features are generally 300−400 nm in diameter (resolution is diffraction limited), and typically ~500 features are observed on a treated cell. It is important to point out that many of the observed bright spots under the Rayleigh light scattering (and subsequently deconvoluted as halo-like features) are typically made up of small clusters of NPs in each bright spot. We were able to gather images on the same cell using Rayleigh light scattering and SERS microscopy and observe good correlation between SERS active sites and regions of higher cluster density in the Rayleigh light scattering (Figure 2g).

Using NP-assisted two-photon luminescence, we are able to obtain wet cell images of fixed cells that show a similar pattern in NP aggregations as those observed with SERS mapping. Noble NPs are capable of generating very efficient multiphoton photoluminescence due to their plasmonic properties.[21,46,47] This allows us to probe the NP-labeled cells with the native two-photon luminescence signature of the Ag NPs. We are able to detect the particles' distribution on the cell surface and observed a very similar pattern to those obtained in SERS and light scattering experiments. In all of these NP-assisted optical imaging techniques, we observed that most particles tend to aggregate toward one region of the cell. The two-photon luminescence images showed that numbers of discrete detectable NP clusters per cell ranged from 500 to 1000 (Figure 4 and Supporting Information, Figure S4), similar to that observed using Rayleigh light scattering. The size of these features as deconvoluted by software is ~300 nm (diffraction limited). There are particles located across the entire cell surface; however, areas of aggregation are typically observed on all cells. Mapping the same cell using two-photon luminescence (Figure 4a,b) and SERS (Figure 4c) microscopy, we were able to generate and superimpose images from the two techniques (Figure 4d). There is a general correlation between SERS active sites and observed particle luminescence; however, the shape of the cell outlines is somewhat different as a result of the drying process used for performing the SERS microscopy. There is a difference in cellular volume and thus surface topography upon drying the cells. This causes the receptors to shift slightly from the positions observed under wet conditions for luminescence. Nevertheless, we were able to correlate the respective signals from NP aggregated in both techniques (Figure 4). The two-photon luminescence microscopy is not per-

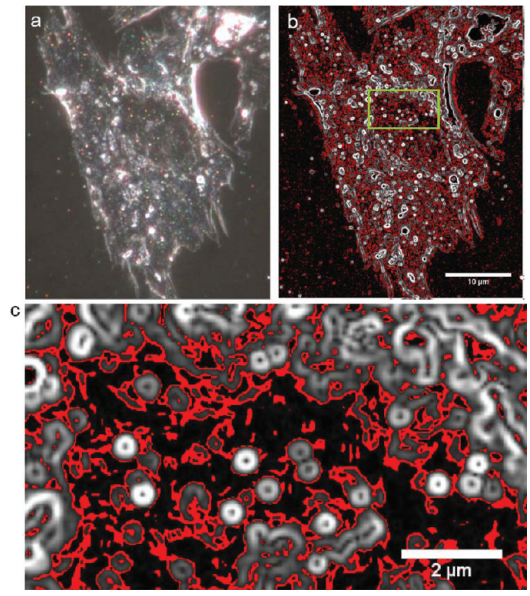

Figure 3. Analysis of Rayleigh light scattering. In order to process the image in (a), the data were converted from color to an 8-bit black and white image using ImageJ software. Then the "defined edges" protocol was used to create an outline for each of the NPs (b). With the edges clearly defined, each spot from NPs appears as a donut. The thresholds for selecting features were set so that black was set to zero (no signal) and red was set one level below the threshold, causing a ringing of features to help identify them more clearly. White spots then set above the threshold were detected for NPs and for salt. The NPs, however, had a characteristic halo shape that can be easily distinguished from the random salt formations (c) and can thus be identified and quantified on the cell surface.

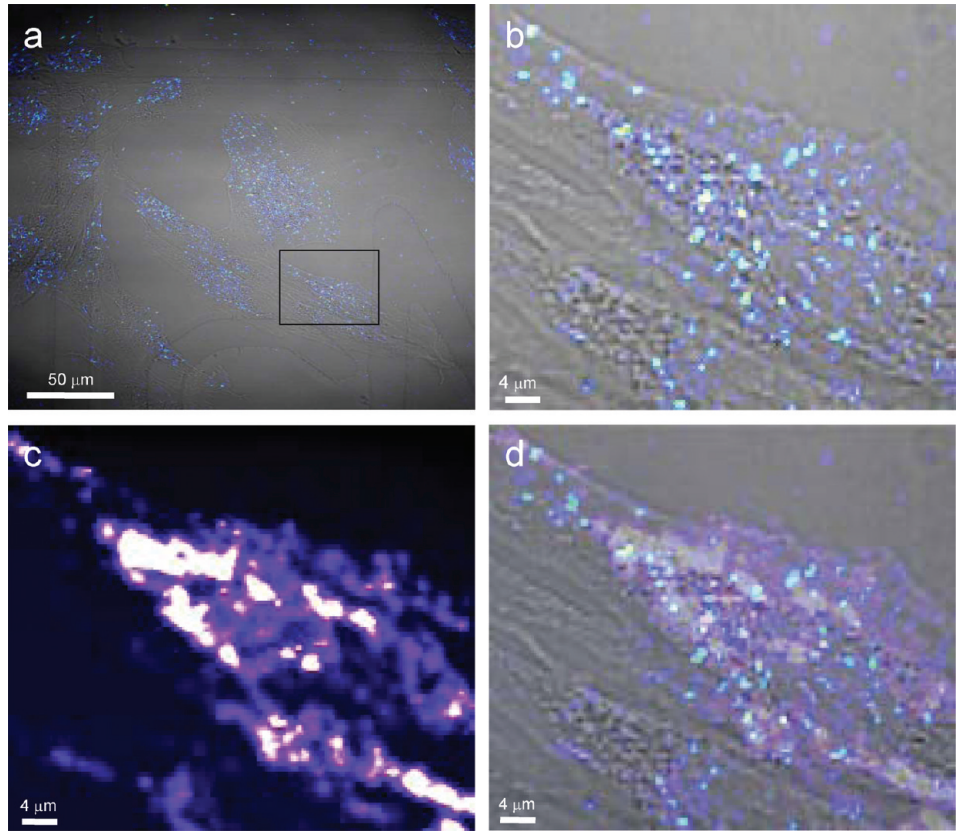

Figure 4. (a) Two-photon luminescent and bright-field image of several fixed H9c2 cells immunostained for β_2AR and co-stained with secondary antibody-functionalized NPs. The cells were fixed and the spectra acquired while still in PBS. (b) Enlarged two-photon luminescence image of a single cell from (a). (c) SERS spectrum acquired for that same cell in (b) after drying the sample. (d) On overlay of (b) and (c), blue/green spots represent NPs, while the white regions are SERS active sites.

formed on the dry samples as the aqueous medium is required to dissipate heat generated by the NPs upon pulse laser excitation. Conversely, the SERS microscopy is performed on dry cells, as contact of a solution with the objective that may contain particles that have dissociated from the cell surface could permanently damage the objective. While there is no evidence for free NPs in solution from the two-photon luminescence, a single particle breaking free from the cell during rinsing would be sufficient to damage the objective.

In order to confirm that SERS active sites were arising from local β_2AR receptor clusters, we obtained a series of high-resolution scanning electron microscopy (SEM) images of a cell that gave rise to the highest resolution images ever obtained of receptor clusters on a cell surface. These were combined to form one high-resolution SEM image of the entire cell that was compared with SERS microscopy of the same cell. SEM, being a surface technique, gives only information on NPs on the extracellular surface, ruling out any contribution from NPs that may have permeated the cell membrane. This would be unexpected in any case as the cells were fixed before treatment with Abs. The overlay of the two images shows excellent correlation of the SERS activity with regional clustering of the NPs (Figure 5a). The SERS intensity map (Figure 5a), shown in purple-white (with the white regions indicating areas of highest SERS intensity), is superimposed on top of the gray scaled SEM images. The bright spots in the high-resolution SEM images indicate the distribution of NPs on the cell surface. The high atomic weight contrast between the Ag NPs and cell materials renders the NPs easily discernible as the small white spots on the surface of the cell. From Figure 5a, intense SERS signals are clearly visible predominantly in the upper left region of the cell, as well as some other NP aggregates surrounding the cell nucleus. The distribution pattern of the NPs as revealed by the SEM images implies that in the upper left region of the cell there is a clustering of NPs arising from a local concentration of cell surface receptors.

Quantifying NP-Labeled Adrenergic Receptor Aggregates on the Cell Surface. The number of NPs located on the cell surface was counted using an automated image analysis counting algorithm. The cell shown in Figure 5a is coated with ~10 000−15 000 functionalized NPs, consistent with the expected number of receptors on the cell surface measured previously.[7] This was determined using an average of 22 pixels per NP as defined by zooming in on regions with very sparsely scattered NPs that could be easily counted and then correlated to the number of pixels above a given threshold value. The range of values results from the uncertainty in selecting a threshold value that excludes all background

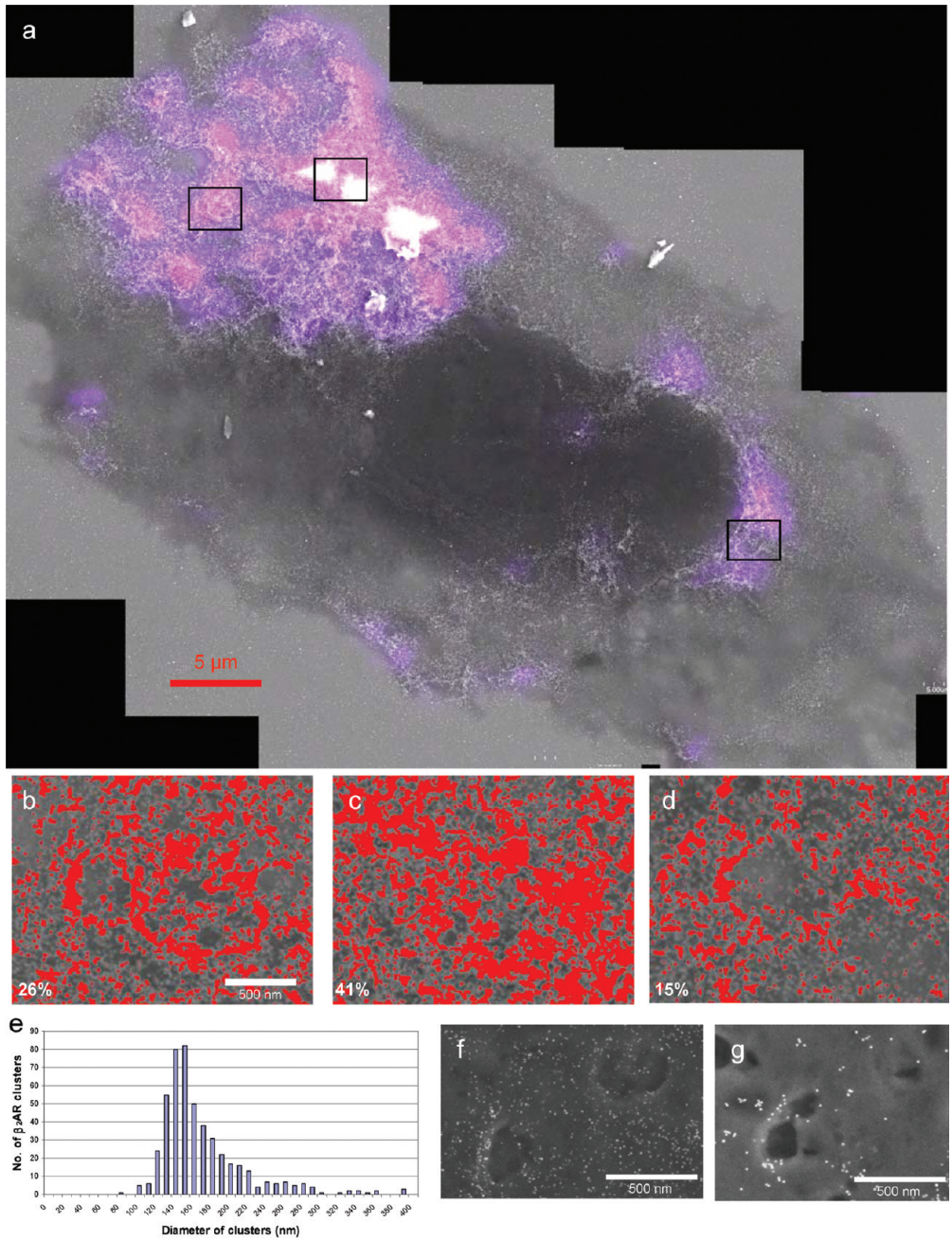

Figure 5. Composite of a high-resolution SEM image of a NP-functionalized cell overlaid with the corresponding SERS map for the same cell. (a) High-resolution SEM image for fixed H9c2 cells immunostained for β_2AR and co-stained with secondary antibody-functionalized NPs. This image is a composite of 34 high-resolution SEM images. (b−d) Three different areas that give rise to SERS signals of variable intensity are shown by smoothing the SEM images to facilitate the visualization of the NPs as clusters. The density of NPs in a region is related to the intensity of the corresponding SERS signal showing the dependence on clustering of NPs required to generate intense SERS signals. (e) Histogram depicting the number of clusters of given sizes as determined by analysis of the smoothed SEM data that were used to generate clusters of NPs. (f,g) Individual high-resolution SEM images of β_2ARs co-stained with secondary antibody-functionalized NPs showing NPs and pitted topographical features.

but includes all particles. Looking at regions where the weakest and strongest SERS signals were detected, we determined that the range of cluster sizes that gave rise to SERS was from 10 to 70 NPs. It is also possible that the brightest features may have benefited from longer range order, where several neighboring clusters were separated from each other by less than 10 nm.

Next we sought to characterize the number of β_2AR aggregates and the number of associated β_2AR molecules per receptor cluster. By smoothing the SEM imaging data, individual particles in the SEM images can be blended into clusters that likely give rise to the SERS signal (Figure 5b−d and Supporting Information, Figure S5; smoothing blends NPs within ~5 nm of each

other into a continuous domain). The clusters range in sizes from 100 to 400 nm in diameter (Figure 5e). As seen in Figure 4b,d, these clusters can be circular in shape; however, the most intense signal arises from a number of very closely packed NPs (Figure 5c). Despite several large domains of NPs, it still appears that the majority of NPs exist in domains of 1−5 NPs that generate weak or undetectable SERS signals. The cluster sizes appear consistent with those previously reported by near-field scanning optical microscopy (NSOM); however, here we are able to gain more information about the smaller nanoscale features that give rise to receptor clusters visualized by near-field microscopy.

SEM image showed that the NPs can be found all over the cell, but the NP aggregates that give rise to observable SERS signature vary in intensity depending on the number of particles associated in a cluster. In addition, the observed MMBN intensity will also depend on factors such as receptor-mediated coupling efficiency between the closely spaced NPs, their orientation with respect to the polarization of the excitation radiation, as well as their local extinction profile.[40] Spectral analysis of the SERS active sites clearly shows the Raman signature for the MMBN-functionalized NPs. Upon closer examination by SEM, NPs on the cell surface appear to form distinct patterns (Figure 5 and Supporting Information, Figure S5). Pitted surface features are often ringed by a higher concentration of particles than other flat parts of the cell surface. In these areas, particles are observed to form single layer arcs or semicircles around these surface features, suggesting that receptors tend to aggregate on the upper lip of these features (Figure 5f,g). What is clear is that there is an exclusion of NPs from these pitted features. This suggests the lack of any receptors associated with the pitted features. There is a high density of receptors scattered across the surface; however, regions of highest density appear to ring around these pitted features and correspond to the SERS active sites. Other random NP distribution scattered over the cell tends to be single or paired particles, suggesting smaller cluster or individual receptors that were generally not observed, similar to our observations by SERS. Only the spots with larger clusters of particles give a strong enough signal to be detected by SERS. These observations are consistent with the notion that β_2AR signaling occurs within distinct membrane domains on the cell surface and that β_2ARs do not readily migrate from these membranous features.

Isopreterenol is an agonist typically used to activate β_2ARs on the cell surface. β_2ARs have been previously imaged by NSOM under resting and isopreterenol activated conditions, and in both cases, the receptor distribution appeared to be random and universal across the cells. Here we also investigated the consequence of such activation using the NP-assisted imaging techniques. In these experiments, cells were treated with isopreterenol before fixation and then treated with both the primary antibody and functionalized NPs. We observed a similar distribution pattern in the receptor distribution as was observed by SERS in the unactivated cells. High-resolution SEM images revealed the same types of features on the cell surface as well with the pitted features being rings by NPs, suggesting a very similar pattern in receptor distribution under both sets of conditions. This finding is consistent with the previous interpretation that signaling clusters are preformed on the cell surface and do not require large lateral diffusion events for efficient signal transduction to occur.

CONCLUSIONS

In conclusion, SERS microscopy can be used to report on the aggregation of β_2ARs using functionalized Ag NPs. The combination of Rayleigh scattering and SERS microscopies provides good validation that the SERS active sites correlate well with the spatial location of the NPs. Similar to SERS, the Rayleigh scattering and two-photon luminescence imaging techniques can validate information on the receptor clustering, with the latter approach providing the possibility for live cell imaging. SEM by far gives the highest resolution images of receptor clusters on the surfaces of cardiac myocytes. SEM studies indicate that approximately 10 000 NPs bind the surface of the cell, and these NPs tend to associate together in localized domains. Aggregates of 10 or more 15 nm Ag NPs often couple to produce an observable SERS signal that is otherwise undetectable for individual particles. Here we have been able to not only identify clusters of receptors on the cell surface but also to determine that cells can exhibit a variety of receptor clustering patterns and that clusters tend to associate together in an ordered or directed manner in order to properly function. Our findings suggest that not all forms of β_2-adrenergic receptor on the cell surface may be functional and nanoscale approaches for their interrogation may help define subpopulations of receptor on the cell surface as future targets for therapeutic intervention.

MATERIALS AND METHODS

Cell Culture. H9c2 cells (ATCC, Manassas, VA) were grown in Dulbecco's modified Eagle's medium (Invitrogen, Burlington, ON) supplemented with 10% fetal bovine serum (FBS) (North-Bio, Toronto, ON) under standard culture conditions (37 °C, 5% CO_2).

Nanoparticle Coatings. The nanoparticles were coated with a mixture of three thiolates. Dithiobis(succinimidyl propionate) (DTSP) was purchased form Aldrich. Reagents for the synthesis of 4-(mercaptomethyl)benzonitrile (MMBN) and 2-(2-(2-methoxyethoxy)ethoxy)ethanethiol (EG_3SH) were also purchased from Aldrich and used as received. EG_3SH was prepared accord-

ing to a known procedure.[33] To synthesize MMBN, 4-(chloromethyl)benzonitrile) (1.0 g) was dissolved in H_2O (15 mL), and to this solution were added thiourea (0.46 g) and NaI (1.0 g). This solution was refluxed for 4 h and then the solvent removed by rotary evaporation. The isolated isothiouronium salt intermediate was then dissolved in dilute aqueous sodium bicarbonate (5 g of $NaHCO_3$ in 25 mL of H_2O). This solution was refluxed for 2 h and then cooled to room temperature. A white precipitate was collected by vacuum filtration. TLC showed only one band that was determined to be the intended product by mass and ^1H NMR spectral analysis.[31]

Nanoparticle Synthesis. Silver NPs were synthesized with the citrate reduction protocol. A solution of $AgNO_3$ (50.0 mL, 1.0 mM) in 18.2 MΩ deionized water was heated until it began to boil. One milliliter of 51.0 mM sodium citrate solution was added to the boiling $AgNO_3$ solution. The color of the solution slowly turned into grayish-yellow. The solution was maintained at boiling condition and under reflux for another 60 min. The Ag sol was cooled to room temperature before storage at 4 °C. To 1 mL of Ag particles (10^{13}/mL) was added 100 μL of 50 mM Na borate buffer (pH = 9) in a glass vial (plastic tubes resulted in particle precipitation during the ligand exchange process). To this was added 4 μL of 2 mM DTSP. After 5 min, 30 μL of 2 mM EG_3SH and 30 μL of 2 mM MMBN were added. The resulting solution was left stirring for 4 h. The pH was then raised by adding 400 μL of 50 mM Na borate buffer (pH = 9). To this solution was added 80 μL of the secondary antibody solution (Affinipure goat antirabbit IgG (H+L), 2.4 mg/mL (Jackson Immunoresearch)), and the resulting solution was mixed by pipetting it slowly several times. This solution was left in the refrigerator at 4 °C overnight (16 h). After 16 h, the solution was warmed to rt and 30 μL of 30% bovine serum albumin (BSA) (Sigma) was added. This solution was mixed with a pipet and left to stand for 30 min at rt. After 30 min, the solution was transferred to a 1.5 mL Eppendorf microcentrifuge tube and spun at 13.4 k rpm for 20 min to pellet the particles. The supernatant was then removed, and the particles were resuspended in 500 μL of PBS. Attempts to pellet and resuspend particles either without BSA blocking or prior to antibody treatment were not successful. The resulting solutions were determined to be approximately 20 nM by UV−vis and were stored at 4 °C. Samples were stable for over 1 month under these conditions. NP solutions could be collected after use and used at least five times before a decrease in effectiveness of labeling was observed.

Sample Preparations for Imaging. H9c2 cells were plated onto photoetched coverslips (Electron Microscopy Sciences, Hatfield, PA) or silicon wafers. After 24 h, the cells were fixed and then rinsed and stored in PBS at 4 °C. The cells were then treated with a primary antibody against the β_2-adrenergic receptor (β_2AR (H-73) rabbit polyclonal IgG (Santa Cruz Biotechnology), 0.2 mg/mL, 4 μL used per mL PBS) for 16 h at 4 °C, then rinsed twice with PBS, and 1 mL of Ag NP solution was added. The cells were incubated with the NP solution for 24 h and then rinsed twice with PBS and twice with water to remove unbound particles as well as salt before imaging. The NP solution was recovered after the 24 h treatment and could be reused for subsequent labeling studies (at least five times).

Surface-Enhanced Raman Scattering Imaging and Spectroscopy. Raman spectroscopy and microscopy was acquired with a commercial microRaman system (LabRAM HR, Horiba Jobin Yvon) equipped with a software controlled XYZ stage and a thermal-electric cooled CCD detector. Samples were excited with 632.8 nm radiation at a power density of ~10^3 W/cm^2. Incident radiation was coupled into an Olympus BX51 optical microscope and focused to ~1 μm diameter spot through a 100× objective. The same objective also collects the retro-reflected radiation and guides it to a notch filter, which removes the Rayleigh radiation. In the Raman mapping experiments, a fine set of grid points within an area of interest is defined in the software and imaged by rastering the sample under the tightly focused laser beam. At each of the grid point, a full Raman spectrum was acquired. SERS images were generated with 1 s acquisition time (two accumulations) with a power density of 10^3 W/cm^2. Cell Raman spectrum (Figure 2b) was acquired with 5 s acquisition time (six accumulations) with a power density of 10^5 W/cm^2. The multiple accumulations are necessary for the spike removal algorithm to function. Upon completion of the mapping, Raman intensity map of the C≡N vibrational mode is regenerated by fitting and removing the associated background for each spectrum in the predefined spatial grid. The C≡N intensity is displayed as a thermal map, as shown in Figures 2c, 4a, and 5a. This is achieved by the Labspec 5.25 software (Horiba Jobin Yvon).

Resonant Rayleigh Imaging. Resonant Rayleigh images of the cells were obtained in two different setups. Figure 2e was obtained using an upright Nikon Eclipse ME600 optical microscope operating in a reflective dark-field optical beam path. Samples were illuminated with a 100 W halogen lamp, and the scattered light was collected by a Nikon Plan Fluor ELWD 100× objective and recorded by a CoolPiX digital camera. A transmission dark-field setup was adapted onto the Olympus BX51 microscope equipped with an oil immersion dark-field condenser (NA = 1.3) and a 100× objective (NA = 0.9). Samples were illuminated with a 75 W xenon lamp and scattered light recorded with an UEye color camera.

Scanning Electron Microscopy. Scanning electron microscopy was performed on cells plated on a Si substrate with a Hitachi S-4700 field-emission scanning electron microscope. Samples were imaged with an acceleration voltage of 3 keV and at a working distance of 12 mm. The high-resolution SEM image of the whole cell shown in Figure 4a was generated from 34 individual high-resolution SEM images, each acquired at a 10 000× magnification. Stitching was performed manually in the image processing software.

Two-Photon Luminescence Imaging. The two-photon luminescence microscopy system uses a single femtosecond Ti:sapphire oscillator (Spectra Physics Tsunami operating at 80 MHz) as the excitation source (800 nm, 15 mW average power). A modified Olympus Fluoview 300 laser scanning system and IX71 inverted microscope were used to carry out the imaging. A 40× 1.15 NA UAPO water immersion lens with a coverslip collection was used as the objective. Light was directed to photomultiplier tubes (PMT) with enhanced red sensitivity (Hamamatsu R3896). Two-photon luminescence images were collected on fixed cell samples on photoetched glass slides that were subsequently inverted and immersed in PBS in 4.2 cm^2 Lab-Tek Chambers Slide System (NUNC, Rochester, NY). The bottom surface of the cells (top from slides) was brought into focus to image the NPs on the surface (no NPs were detected inside the cell). Bright-field images were collected simultaneously in order to define the border outlines of cells.

Acknowledgment. We thank A. Stolow and A. Ridsdale for assistance with two-photon luminescence experiments. We gratefully acknowledge J. Fraser for the high-resolution SEM imaging, and X. Wu for the TEM imaging of Ag nanoparticles. This work was supported by a grant from the Canadian Institutes of Health Research (CIHR).

Supporting Information Available: Analytical data, additional images, and description of data analysis are available. This material is available free of charge *via* the Internet at http://pubs.acs.org.

REFERENCES AND NOTES

1. Davare, M. A.; Avdonin, V.; Hall, D. D.; Peden, E. M.; Burette, A.; Weinberg, R. J.; Horne, M. C.; Hoshi, T.; Hell, J. W. A β2 Adrenergic Receptor Signaling Complex Assembled with the Ca^{2+} Channel $Ca_v1.2$. *Science* **2001**, *293*, 98–101.
2. Hall, R. A.; Lefkowitz, R. J. Regulation of G-Protein-Coupled Receptor Signaling by Scaffold Proteins. *Circ. Res.* **2002**, *91*, 672–680.
3. Razani, B.; Woodman, S. E.; Lisanti, M. P. Caveolae: From Cell Biology to Animal Physiology. *Pharmacol. Rev.* **2002**, *54*, 431–467.
4. Rybin, V. O.; Xu, X. H.; Lisanti, M. P.; Steinberg, S. F. Differential Targeting of Beta-Adrenergic Receptor Subtypes and Adenylyl Cyclase to Cardiomyocyte Caveolae—A Mechanism to Functionally Regulate the cAMP Signaling Pathway. *J. Biol. Chem.* **2000**, *275*, 41447–41457.

5. Coulon, V.; Audet, M.; Homburger, V.; Bockaert, J.; Fagni, L.; Bouvier, M.; Perroy, J. Subcellular Imaging of Dynamic Protein Interactions by Bioluminescence Resonance Energy Transfer. *Biophys. J.* **2008**, *94*, 1001–1009.
6. Richter, W.; Day, P.; Agrawal, R.; Bruss, M. D.; Granier, S.; Wang, Y. L.; Rasmussen, S. G. F.; Horner, K.; Wang, P.; Lei, T.; Patterson, A. J.; Kobilka, B.; Conti, M. Signaling from β_1- and β_2-Adrenergic Receptors is Defined by Differential Interactions with PDE4. *EMBO J.* **2008**, *27*, 384–393.
7. Ianoul, A.; Grant, D. D.; Rouleau, Y.; Bani-Yaghoub, M.; Johnston, L. J.; Pezacki, J. P. Imaging Nanometer Domains of β-Adrenergic Receptor Complexes on the Surface of Cardiac Myocytes. *Nat. Chem. Biol.* **2005**, *1*, 196–202.
8. Bouvier, M. Oligomerization of G-Protein-Coupled Transmitter Receptors. *Nat. Rev. Neurosci.* **2001**, *2*, 274–286.
9. Rockman, H. A.; Koch, W. J.; Lefkowitz, R. J. Seven-Transmembrane-Spanning Receptors and Heart Function. *Nature* **2002**, *415*, 206–212.
10. Dorsch, S.; Klotz, K. N.; Engelhardt, S.; Lohse, M. J.; Bunemann, M. Analysis of Receptor Oligomerization by FRAP Microscopy. *Nat. Methods* **2009**, *6*, 225–230.
11. Cherezov, V.; Rosenbaum, D. M.; Hanson, M. A.; Rasmussen, S. G.; Thian, F. S.; Kobilka, T. S.; Choi, H. J.; Kuhn, P.; Weis, W. I.; Kobilka, B. K.; Stevens, R. C. High-Resolution Crystal Structure of an Engineered Human β_2-Adrenergic G Protein-Coupled Receptor. *Science* **2007**, *318*, 1258–1265.
12. Rasmussen, S. G.; Choi, H. J.; Rosenbaum, D. M.; Kobilka, T. S.; Thian, F. S.; Edwards, P. C.; Burghammer, M.; Ratnala, V. R.; Sanishvili, R.; Fischetti, R. F.; Schertler, G. F.; Weis, W. I.; Kobilka, B. K. Crystal Structure of the Human β_2 Adrenergic G-Protein-Coupled Receptor. *Nature* **2007**, *450*, 383–387.
13. Rosenbaum, D. M.; Cherezov, V.; Hanson, M. A.; Rasmussen, S. G.; Thian, F. S.; Kobilka, T. S.; Choi, H. J.; Yao, X. J.; Weis, W. I.; Stevens, R. C.; Kobilka, B. K. GPCR Engineering Yields High-Resolution Structural Insights into β_2-Adrenergic Receptor Function. *Science* **2007**, *318*, 1266–1273.
14. Nakanishi, J.; Takarada, T.; Yunoki, S.; Kikuchi, Y.; Maeda, M. FRET-Based Monitoring of Conformational Change of the β_2 Adrenergic Receptor in Living Cells. *Biochem. Biophys. Res. Commun.* **2006**, *343*, 1191–1196.
15. Angers, S.; Salahpour, A.; Joly, E.; Hilairet, S.; Chelsky, D.; Dennis, M.; Bouvier, M. Detection of β_2-Adrenergic Receptor Dimerization in Living Cells Using Bioluminescence Resonance Energy Rransfer (BRET). *Proc. Natl. Acad. Sci. U.S.A.* **2000**, *97*, 3684–3689.
16. Salahpour, A.; Bonin, H.; Bhalla, S.; Petaja-Repo, U.; Bouvier, M. Biochemical Characterization of β_2-Adrenergic Receptor Dimers and Oligomers. *Biol. Chem.* **2003**, *384*, 117–123.
17. Salahpour, A.; Angers, S.; Mercier, J. F.; Lagace, M.; Marullo, S.; Bouvier, M. Homodimerization of the β_2-Adrenergic Receptor as a Prerequisite for Cell Surface Targeting. *J. Biol. Chem.* **2004**, *279*, 33390–33397.
18. Breit, A.; Lagace, M.; Bouvier, M. Hetero-Oligomerization between β_2- and β_3-Adrenergic Receptors Generates a β-Adrenergic Signaling Unit with Distinct Functional Properties. *J. Biol. Chem.* **2004**, *279*, 28756–28765.
19. Vobornik, D.; Rouleau, Y.; Haley, J.; Bani-Yaghoub, M.; Taylor, R.; Johnston, L. J.; Pezacki, J. P. Nanoscale Organization of Beta2-Adrenergic Receptor—Venus Fusion Protein Domains on the Surface of Mammalian Cells. *Biochem. Biophys. Res. Commun.* **2009**, *382*, 85–90.
20. Cao, Y. W. C.; Jin, R. C.; Mirkin, C. A. Nanoparticles with Raman Spectroscopic Fingerprints for DNA and RNA Detection. *Science* **2002**, *297*, 1536–1540.
21. Durr, N. J.; Larson, T.; Smith, D. K.; Korgel, B. A.; Sokolov, K.; Ben-Yakar, A. Two-Photon Luminescence Imaging of Cancer Cells Using Molecularly Targeted Gold Nanorods. *Nano Lett.* **2007**, *7*, 941–945.
22. Hurst, S. J.; Hill, H. D.; Mirkin, C. A. "Three-Dimensional Hybridization" with Polyvalent DNA—Gold Nanoparticle Conjugates. *J. Am. Chem. Soc.* **2008**, *130*, 12192–12200.
23. Kneipp, J.; Kneipp, H.; Kneipp, K. SERS: A Single-Molecule and Nanoscale Tool for Bioanalytics. *Chem. Soc. Rev.* **2008**, *37*, 1052–1060.
24. Kneipp, K.; Kneipp, H.; Kneipp, J. Surface-Enhanced Raman Scattering in Local Optical Fields of Silver and Gold Nanoaggregatess—From Single-Molecule Raman Spectroscopy to Ultrasensitive Probing in Live Cells. *Acc. Chem. Res.* **2006**, *39*, 443–450.
25. Qian, X. M.; Nie, S. M. Single-Molecule and Single-Nanoparticle SERS—From Fundamental Mechanisms to Biomedical Applications. *Chem. Soc. Rev.* **2008**, *37*, 912–920.
26. Roca, M.; Haes, A. J. Probing Cells with Noble Metal Nanoparticle Aggregates. *Nanomedicine* **2008**, *3*, 555–565.
27. Hu, Q.; Tay, L. L.; Noestheden, M.; Pezacki, J. P. Mammalian Cell Surface Imaging with Nitrile-Functionalized Nanoprobes: Biophysical Characterization of Aggregation and Polarization Anisotropy in SERS Imaging. *J. Am. Chem. Soc.* **2007**, *129*, 14–15.
28. Huang, X.; El-Sayed, I. H.; Qian, W.; El-Sayed, M. A. Cancer Cells Assemble and Align Gold Nanorods Conjugated to Antibodies to Produce Highly Enhanced, Sharp, and Polarized Surface Raman Spectra: A Potential Cancer Diagnostic Marker. *Nano Lett.* **2007**, *7*, 1591–1597.
29. Suydam, I. T.; Snow, C. D.; Pande, V. S.; Boxer, S. G. Electric Fields at the Active Site of an Enzyme: Direct Comparison of Experiment with Theory. *Science* **2006**, *313*, 200–204.
30. Noestheden, M.; Hu, Q.; Tay, L. L.; Tonary, A. M.; Stolow, A.; MacKenzie, R.; Tanha, J.; Pezacki, J. P. Synthesis and Characterization of CN-Modified Protein Analogues as Potential Vibrational Contrast Agents. *Bioorg. Chem.* **2007**, *35*, 284–293.
31. Szafranski, C. A.; Tanner, W.; Laibinis, P. E.; Garrell, R. L. Surface-Enhanced Raman Spectroscopy of Aromatic Thiols and Disulfides on Gold Electrodes. *Langmuir* **1998**, *14*, 3570–3579.
32. Friedrich, M. G.; Kirste, V. U.; Zhu, J.; Gennis, R. B.; Knoll, W.; Naumann, R. L. Activity of Membrane Proteins Immobilized on Surfaces as a Function of Packing Density. *J. Phys. Chem. B* **2008**, *112*, 3193–3201.
33. Zheng, M.; Li, Z.; Huang, X. Ethylene Glycol Monolayer Protected Nanoparticles: Synthesis, Characterization, and Interactions with Biological Molecules. *Langmuir* **2004**, *20*, 4226–4235.
34. Socrates, G., *Infrared and Raman Characteristics Group Frequencies, Tables and Charts*, 3rd ed.; John Wiley and Sons Ltd.: Toronto, 2005.
35. Anker, J. N.; Hall, W. P.; Lyandres, O.; Shah, N. C.; Zhao, J.; Van Duyne, R. P. Biosensing with Plasmonic Nanosensors. *Nat. Mater.* **2008**, *7*, 442–453.
36. McFarland, A. D.; Young, M. A.; Dieringer, J. A.; Van Duyne, R. P. Wavelength-Scanned Surface-Enhanced Raman Excitation Spectroscopy. *J. Phys. Chem. B* **2005**, *109*, 11279–11285.
37. Willets, K. A.; Van Duyne, R. P. Localized Surface Plasmon Resonance Spectroscopy and Sensing. *Annu. Rev. Phys. Chem.* **2007**, *58*, 267–297.
38. Zhu, W. Z.; Chakir, K.; Zhang, S.; Yang, D.; Lavoie, C.; Bouvier, M.; Hebert, T. E.; Lakatta, E. G.; Cheng, H.; Xiao, R. P. Heterodimerization of β_1- and β_2-Adrenergic Receptor Subtypes Optimizes β-Adrenergic Modulation of Cardiac Contractility. *Circ. Res.* **2005**, *97*, 244–251.
39. Qian, X.; Peng, X. H.; Ansari, D. O.; Yin-Goen, Q.; Chen, G. Z.; Shin, D. M.; Yang, L.; Young, A. N.; Wang, M. D.; Nie, S. *In Vivo* Tumor Targeting and Spectroscopic Detection with Surface-Enhanced Raman Nanoparticle Tags. *Nat. Biotechnol.* **2008**, *26*, 83–90.
40. Xu, H.; Bjerneld, E. J.; Kall, M.; Borjesson, L. Spectroscopy of Single Hemoglobin Molecules by Surface Enhanced Raman Scattering. *Phys. Rev. Lett.* **1999**, *83*, 4357–4360.
41. Day, P. W.; Rasmussen, S. G.; Parnot, C.; Fung, J. J.; Masood, A.; Kobilka, T. S.; Yao, X. J.; Choi, H. J.; Weis, W. I.; Rohrer,

D. K.; Kobilka, B. K. A Monoclonal Antibody for G Protein-Coupled Receptor Crystallography. *Nat. Methods* **2007**, *4*, 927–929.
42. Yang, E. V.; Sood, A. K.; Chen, M.; Li, Y.; Eubank, T. D.; Marsh, C. B.; Jewell, S.; Flavahan, N. A.; Morrison, C.; Yeh, P. E.; Lemeshow, S.; Glaser, R. Norepinephrine Up-Regulates the Expression of Vascular Endothelial Growth Factor, Matrix Metalloproteinase (MMP)-2, and MMP-9 in Nasopharyngeal Carcinoma Tumor Cells. *Cancer Res.* **2006**, *66*, 10357–10364.
43. Yguerabide, J.; Yguerabide, E. E. Light-Scattering Submicroscopic Particles as Highly Fluorescent Analogs and Their Use as Tracer Labels in Clinical and Biological Applications. *Anal. Biochem.* **1998**, *262*, 157–176.
44. Liu, G. L.; Yin, Y.; Kunchakarra, S.; Mukherjee, B.; Gerion, D.; Jett, S. D.; Bear, D. G.; Gray, J. W.; Alivisatos, A. P.; Lee, L. P.; Chen, F. F. A Nanoplasmonic Molecular Ruler for Measuring Nuclease Activity and DNA Footprinting. *Nat. Nanotechnol.* **2006**, *1*, 47–52.
45. Sonnichsen, C.; Reinhard, B. M.; Liphardt, J.; Alivisatos, A. P. A Molecular Ruler Based on Plasmon Coupling of Single Gold and Silver Nanoparticles. *Nat. Biotechnol.* **2005**, *23*, 741–745.
46. Wang, H.; Huff, T. B.; Zweifel, D. A.; He, W.; Low, P. S.; Wei, A.; Cheng, J. X. *In Vitro* and *In Vivo* Two-Photon Luminescence Imaging of Single Gold Nanorods. *Proc. Natl. Acad. Sci. U.S.A.* **2005**, *102*, 15752–15756.
47. Moskovits, M. Surface-Enhanced Spectroscopy. *Rev. Mod. Phys.* **1985**, *57*, 783–826.